Robust Distributed Averaging Frequency Control of Inverter-Based Microgrids

Christoph Kammer, Alireza Karimi

***Abstract*— We consider the problem of distributed primary and secondary frequency control in inverter-based microgrids with meshed topology. A dynamic phasor modeling approach is presented that accurately represents the dynamics of the grid while being suitably simple to be used in control design. Then, we propose a novel frequency-domain, fixed structure, multivariable control design method based on a convex approximation of quadratic constraints. The method is then used to design a distributed controller for primary and secondary frequency control in an inverter-based distribution grid that guarantees stability and satisfies various performance goals.**

I. INTRODUCTION

The steady increase of renewable and distributed energy resources in electric power grids is presenting a significant challenge for the stability and reliability of the future electrical network. The classical layout of the electrical grid with few, centralized generation units connected at the high-voltage level is replaced by a new structure, where many small, distributed generation (DG) units are connected to the mid- or low-voltage level. Also, whereas traditional power plants consist of large synchronous generators (SGs), distributed source are often connected through voltage source inverters (VSIs), which exhibit completely different physical characteristics and require new control strategies [1], [2].

The control objective in power grids is to keep the electrical frequency and voltage magnitude at every bus within a close band around the nominal operating point. The control hierarchy of power grids can roughly be separated into three levels, distinguished by a decreasing bandwidth [3], [4]. The primary control level guarantees the short-term stability of the grid. In today's grid this task is performed by droop control, a decentralized, proportional controller. The secondary control level compensates for the steady-state error introduced by primary control, thus keeping the frequency at the nominal value. The current solution is to have a centralized PI-controller that generates an area control signal (ACE), which is broadcast to all generation units participating in secondary control. Finally, the tertiary control level is concerned with the planning and dispatch of reserves during long-lasting disruptions. In this paper we will focus on the primary and secondary levels.

In this work, we would like to address the separation of primary and secondary control, and explore a different approach. A prominent issue is the necessary separation of timescales, which severely limits the bandwidth of secondary control. This in turn decreases the secondary control performance, which presents a problem especially in low-inertia or inverter-only grids with highly stochastic generation. Most works in the literature focus on the case of islanded microgrids consisting solely of VSI-interfaced generation. First attempts usually treated centralized secondary control approaches [5], [6]. However, centralized architectures have the disadvantage that they require all-to-all communication and create a single point of failure. Therefore, recently there has been an effort to develop distributed control schemes that are robust to disturbance and loss of communication. Several distributed controller architectures have been proposed to merge primary and secondary control while retaining power sharing [7], [8], [9]. However, these works do not provide a method to rigorously design the controller parameters for arbitrary grids while guaranteeing stability and satisfy desired performance goals.

From a control perspective, it has only recently been proven that droop control stabilizes the closed-loop system under some assumptions [7], [10]. However, these works use a quasi-static formulation of the power flows, which leads to the inaccurate conclusion that the system is stable for arbitrary droop gains. Therefore, the presented methods are not suitable for control design. A push for rigorous control design for low-inertia power grids is made in [11], but the presented method remains on a very basic level. In [12] a convex robust control design method for distributed voltage controllers for inverter-interfaced grids was presented. A disadvantage of the method is that it uses a time-domain approach based on auxiliary Lyapunov matrices and does not scale well for larger grids.

The contribution of this work is split into two parts. First, in Section II a framework for a dynamic model of an inverter-based, islanded microgrid using a dynamic phasor approach will be presented. This allows to construct a model that accurately represents the electromagnetic and electromechanic dynamics of the grid, while having a significantly reduced complexity compared to a small-signal model. While this type of model has been used for stability analysis and control design of single inverters [13], [14], its application to control design has not been explored so far.

Then, using the dynamic phasor model, in Section III the design of a distributed secondary controller is formulated as an H_∞ control problem. As the second contribution, a novel frequency-domain fixed-structure control approach is proposed in order to solve the design problem. The approach is based on a convex approximation of the frequency-domain

The work presented in this paper was supported by the Swiss Federal Commission for Innovation and Technology within the SCCER-FURIES.

C. Kammer and A. Karimi are with the Laboratoire d' Automatique, École Polytechnique Fédérale de Lausanne, 1015 Lausanne, Switzerland. Corresponding author: alireza.karimi@epfl.ch

constraints and results in a convex formulation of the optimization problem. A notable advantage of the proposed method is that only the frequency response of the plant is required, and there is no need for a parametric model.

II. Grid Model

In this section a linear, dynamic model for an islanded microgrid will be developed that is suitable to be used for the control design task. For stability analysis, power grids are commonly modeled as small signal models. However, this type of model becomes prohibitively complex even for medium-sized grids and is not suitable for control design. One possible solution is to use reduced-order small signal models, but as this approach neglects the transient dynamics, the results are not satisfactory for fast, inverter-based grids. We therefore chose to use a dynamic phasor model that is able to accurately describe the transient dynamics of the bus voltages and power flows while having a significantly reduces complexity compared to the full small-signal model.

Dynamic phasor models for distribution-level grids with a large amount of VSI-interfaced generation are not commonly used so far. In [13] a dynamic phasor model of an inverter-based microgrid is analyzed, however, no load model is given. In the following sections we will describe the models of various grid components, and illustrate how they can be used to form a plant model that can be used in control design. For this work we restrict ourselves to mostly inductive grids and only model the relationship between grid frequency and active power. The voltage magnitude is assumed constant and its dynamics are neglected.

A. Dynamic Line Model

First, we will present the model of the power lines. The balanced, three-phase voltage at bus i is represented in the phasor notation:

$$U_i \angle \theta_i = \sqrt{2} U_i(t) \begin{bmatrix} cos(\bar{\omega} t + \theta_i(t)) \\ cos(\bar{\omega} t + \theta_i(t) - 2\pi/3) \\ cos(\bar{\omega} t + \theta_i(t) + 2\pi/3) \end{bmatrix} \quad (1)$$

with θ_i, U_i being the voltage angle and line-to-ground RMS magnitude at bus i, and $\bar{\omega}$ being the nominal grid frequency. Now consider the simple model shown in Fig. 1 that is commonly used to represent short transmission lines in MV and LV grids. The dynamic formulation of the transfer functions between voltage angle and active power flow P_{ij} transmitted from bus i to bus j is [14]:

$$P_{ij} = 3 \frac{\bar{\omega} L_{ij}}{(L_{ij} s + R_{ij})^2 + (\bar{\omega} L_{ij})^2} \bar{U}^2 \theta_{ij} \quad (2)$$

with R_{ij}, L_{ij} the resistance and inductance of the line, $\bar{U}$ the nominal line-to-ground voltage magnitude and $\theta_{ij} = \theta_i - \theta_j$ the voltage angle difference. The steady-state value of these transfer functions when neglecting the resistive part is equal to the quasi-static formulation commonly used in power flow analysis:

$$P_{ij} = \frac{\bar{U}^2}{X} \theta_{ij} \quad (3)$$

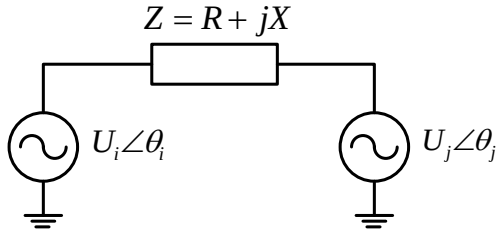

Fig. 1: Single-line diagram of a three-phase transmission line.

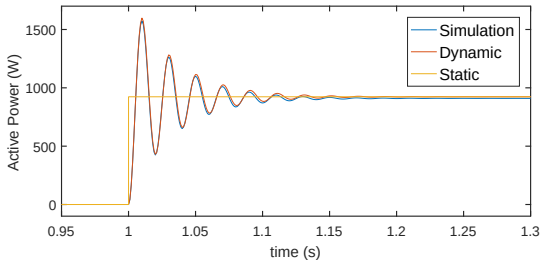

Fig. 2: Comparison of active power flow through a mostly inductive line for complete simulated model, dynamic phasor model and static model.

However, the addition of the second-order dynamics leads to a much more accurate representation of the transient power flows, as can be seen in Fig. 2 after a step of the angle difference at 1 s. One can see significant transient oscillations occuring after stepping up the angle and magnitude difference, which are not represented in the static model. Modeling these oscillations is important especially for VSI control design, since VSIs have a large closed-loop bandwidth and are easily able to excite this resonance.

B. Voltage Source Inverter

VSIs are usually operated in one of two main modes: grid-forming or grid-feeding. In the grid-forming mode, the output voltage is directly controlled to follow a reference given by the operator. This mode is e.g. used to emulate the inertia of a synchronous generator by adjusting the frequency depending on the output power. In the grid-feeding mode, the inverter electrical output power is controlled, with the power setpoints again being provided by the operator.

The dynamic phasor model has the advantage that the complex dynamics introduced by the output filter and internal control loops can be neglected, as only the dynamics between the reference input and the inverter output are required. In this work we will only consider grid-forming inverters. A grid-forming inverter connected to bus i can be represented by the transfer function: $\theta_i = (\tau_{\theta,i} s + 1)^{-1} \bar{\theta}_i$ with $\bar{\theta}_i$ being the desired output voltage angle and $\tau_{\theta,i}$ corresponding to the closed-loop bandwidth of the inverter.

C. Static Active Power Loads

In this work we only consider constant active power loads:

$$P_i = a_i \bar{P}_i \quad (4)$$

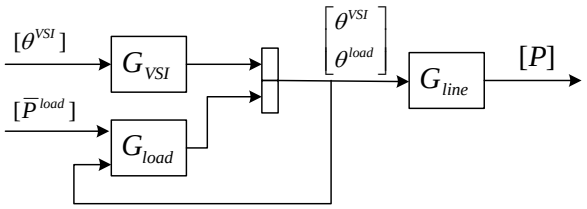

Fig. 3: Block diagram of the plant.

where $P_i, \bar{P}_i$ are the actual and nominal active power drawn by the load and a_i is a load parameter. It is also assumed that the power consumed by a load at bus i is always equal to the power transmitted through the lines connected to bus i. Using the power flow equation presented above, this leads to the following transfer function:

$$P_i = \sum_{j\in\Omega} 3\frac{\bar{\omega}L_{ji}}{(L_{ji}s + R_{ji})^2 + (\bar{\omega}L_{ji})^2}\bar{U}^2(\theta_j - \theta_i) \quad (5)$$

with Ω being the set of all buses j physically connected to bus i. Rewriting this equation gives us the following transfer function for the load bus voltage angle θ_i:

$$\sum_{j\in\Omega} 3\frac{\bar{\omega}L_{ji}}{(L_{ji}s + R_{ji})^2 + (\bar{\omega}L_{ji})^2}\bar{U}^2\theta_i = \quad (6)$$
$$-a_i\bar{P}_i + \sum_{j\in\Omega} 3\frac{\bar{\omega}L_{ji}}{(L_{ji}s + R_{ji})^2 + (\bar{\omega}L_{ji})^2}\bar{U}^2\theta_j$$

D. Block Diagram

Let the superscripts $(\cdot)^{\text{VSI}}, (\cdot)^{\text{load}}$ denote the sets of buses to which a VSI or a load is connected respectively. As an example: if n is the number of inverters in the grid, $\theta^{\text{VSI}} = [\theta_1, \ldots, \theta_n]^T$ would be a vector containing the voltage angles at every bus belonging to a VSI. The block diagram of the dynamic phasor model of a power grid with VSIs and constant active power loads is shown in Fig. 3. The blocks $G_{\text{line}}, G_{\text{VSI}}, G_{\text{load}}$ represent the transfer function matrices containing the grid component models.

III. Distributed Secondary Control

In current power grids, secondary control is based on a centralized integral controller architecture and its bandwidth is limited by the primary control level due to the necessary separation of timescales. This reduces the available performance, an issue that is enhanced in grids with a high amount of stochastic generation, which leads to large and frequent deviations from the nominal frequency. This in turn undermines grid stability and can lead to more frequent disruptions. The work in [7] proposes a distributed-averaging proportional-integral (DAPI) controller which is combining droop control and secondary control. This makes it possible to operate with the same bandwidth as droop control while eliminating the steady-state error and maintaining proportional power sharing. However, the authors do not provide a method to design the control parameters to guarantee that closed-loop stability and other desired performance goals are satisfied. In this section we will reformulate the DAPI controller in a state-space form such that it can be used in the proposed control design method, and calculate feasible integral gains such that the system remains stable and the integral action has an acceptable bandwidth.

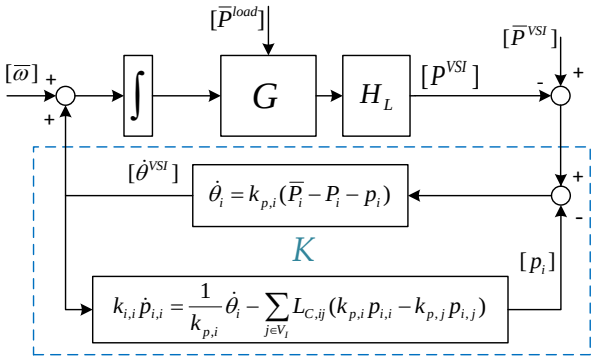

Fig. 4: Block diagram of the closed-loop system with the DAPI controller.

A. DAPI Controller Formulation

Let n be the number of inverters in the grid, and let I_n be the $n \times n$ identity matrix. The DAPI controller of a VSI at bus i is formulated as follows:

$$\dot{\theta}_i = k_{p,i}(\bar{P}_i - P_i - p_{i,i}), \quad i = 1, \ldots, n \quad (7)$$
$$k_{i,i}\dot{p}_{i,i} = \frac{1}{k_{p,i}}\dot{\theta}_i + \sum_j L_{c,ij}(k_{p,i}p_{i,i} - k_{p,j}p_{i,j})$$

where $k_{p,i}, k_{i,i}$ are the proportional and integral gains, $\bar{P}_i, P_i$ are the nominal and measured power of the VSI, and $L_c \in \mathbb{R}^{n\times n}$ is the Laplacian matrix corresponding to a weighted, undirected and connected communication graph between all VSIs in the grid. The first equation is analogous to a classical droop controller, with $k_{p,i}$ being the droop gains. The additional term $p_{i,i}$ serves to take on the role of secondary control, while the distributed architecture ensures that proportional power sharing is maintained.

A block diagram of the full system is shown in Fig. 4. The transfer function matrix G is the single-block formulation of the plant shown in Fig. 3. $\left[P^{\text{VSI}}\right]$ is a vector containing the active power drawn from the VSIs, and the nominal power drawn by the loads $\left[\bar{P}^{\text{load}}\right]$ enters the plant as a disturbance. H_L is the transfer function matrix of the sensor taking the power measurements. Next, the controller will be rewritten in a state-space form. First, let us define state x, input e and output u as:

$$x = \begin{bmatrix} p_{i,1} \\ p_{i,2} \\ \vdots \\ p_{i,n} \end{bmatrix}, \quad e = \begin{bmatrix} \bar{P}_1 - P_1 \\ \bar{P}_2 - P_2 \\ \vdots \\ \bar{P}_n - P_n \end{bmatrix}, \quad u = \begin{bmatrix} \dot{\theta}_1 \\ \dot{\theta}_2 \\ \vdots \\ \dot{\theta}_n \end{bmatrix} \quad (8)$$

The controller equations can then be rewritten as:

$$K_I\dot{x} = -I_n x - L_c K_P x + I_n e \quad (9)$$
$$u = -K_P x + K_P e$$

with K_P, K_I being diagonal matrices with $\text{diag}(K_P) = [k_{p,1}, \ldots, k_{p,n}]$ and $\text{diag}(K_I) = [k_{i,1}, \ldots, k_{i,n}]$. This leads to the state-space form:

$$K = C(sK_I - A)^{-1}B + D \tag{10}$$

with

$$\begin{array}{ll} A = -L_c K_P - I & B = I \\ C = -K_P & D = K_P \end{array} \tag{11}$$

B. Control Design

For the subsequent controller design, the proportional gain matrix K_P is assumed to be known, with the entries being equal to the droop gains of the individual VSIs. Let $\mathcal{U} = K(I+GK)^{-1}$ be the input sensitivity and $\mathcal{S} = (I+GK)^{-1}$ be the sensitivity transfer function. The control objective is to design the integral gains such that the system remains stable and that the VSI frequencies return to the nominal value within a short amount of time after a change in the VSI reference or output power. Due to the frequencies being the input of the plant, this leads to a very specific case that differs from the standard formulation. When looking at the block diagram in Fig 4, the control objective can be formulated as minimizing the norm of the input sensitivity at low frequencies up to a certain point. An additional constraint on the maximum norm of the sensitivity serves to prevent large transient oscillations.

For a $p \times q$ stable transfer function H, the infinity-norm is defined as: $\|H\|_\infty = \sup_{\omega \geq 0} \|H(j\omega)\|$. The control design problem is then formulated as an optimization problem with the integral gain matrix K_I as optimization variable:

$$\begin{aligned} &\min_{K_I} \quad \gamma_u \\ &\text{subject to:} \\ &\|W\mathcal{U}\|_\infty < \gamma_u \\ &\|\mathcal{S}\|_\infty \leq \gamma_s, \end{aligned} \tag{12}$$

where γ_u is a scalar variable, γ_s is a scalar constant and $W(j\omega)$ is a weighting frequency function. The control problem is to compute the diagonal matrix K_I with constraints on the infinity norm of the closed-loop transfer functions.

This problem is known as a fixed-structure H_∞ control problem which is a theoretically challenging open problem in the control theory. Although, there is no exact solution to this problem, some approximative methods based on non-smooth optimization algorithms have been developed [15] and are available in the Robust Control Toolbox of MATLAB and the open source toolbox HIFOO [16]. In this paper we develop a new method to solve this problem based on a convex approximation of the constraints in the frequency domain, where no parametric model is required.

Let the norm of $W\mathcal{U}$ at each frequency be defined as:

$$\|W\mathcal{U}(j\omega)\| = \sigma_{\max}[W\mathcal{U}(j\omega)] \tag{13}$$

where $\sigma_{\max}(\cdot)$ is the maximum singular value of a matrix. Then, the H_∞ constraint $\|W\mathcal{U}\|_\infty < \gamma_u$ can be represented by the following matrix inequalities if $W\mathcal{U}$ is stable:

$$\left[WK(I+GK)^{-1}\right]^* \left[WK(I+GK)^{-1}\right] \prec \gamma_u^2 I \qquad \forall\omega \tag{14}$$

where $(\cdot)^*$ represents the complex conjugate transpose of a matrix and the argument $j\omega$ is dropped for the ease of notation. This matrix inequality can be written as

$$K^*W^*WK \prec \gamma_u^2 (I+GK)^*(I+GK) \quad \forall\omega \tag{15}$$

Multiplying both sides of the inequality from the left by $(j\omega K_I - A)^*$ and from the right by $(j\omega K_I - A)$, we obtain:

$$Y^*\gamma_u^{-2}Y \prec Z^*Z \qquad \forall\omega \tag{16}$$

where

$$\begin{aligned} Y &= WK(j\omega K_I - A) \\ &= W[C + D(j\omega K_I - A)] \\ Z &= (I+GK)(j\omega K_I - A) \\ &= (I+GD)(j\omega K_I - A) + GC \end{aligned} \tag{17}$$

Note that Y and Z are linear with respect to the optimization variable K_I and so the quadratic matrix inequality in (16) represents the sum of a convex and a concave constraint. The concave part can be linearized starting from the following matrix inequality [17]:

$$0 \preceq (Z - \widetilde{Z})^*(Z - \widetilde{Z}) = Z^*Z - Z^*\widetilde{Z} - \widetilde{Z}^*Z + \widetilde{Z}^*\widetilde{Z} \tag{18}$$

which is valid for any matrices Z and $\widetilde{Z}$. It leads to:

$$Z^*Z \succeq Z^*\widetilde{Z} + \widetilde{Z}^*Z - \widetilde{Z}^*\widetilde{Z} \tag{19}$$

with the right-hand side being an affine function of Z. From this directly follows that:

$$Z^*\widetilde{Z} + \widetilde{Z}^*Z - \widetilde{Z}^*\widetilde{Z} - Y^*\gamma_u^{-2}Y \succ 0 \tag{20}$$

which is convex in Z and Y and poses a sufficient condition for $Z^*Z \succeq Y^*\gamma_u^{-2}Y$. This leads us to the following convex optimization problem with LMI constraints:

$$\begin{aligned} &\min_{K_I} \qquad \gamma_u^2 \\ &\text{subject to} \quad \begin{bmatrix} Z^*\widetilde{Z} + \widetilde{Z}^*Z - \widetilde{Z}^*\widetilde{Z} & Y^* \\ Y & \gamma_u^2 I \end{bmatrix} \succ 0, \quad \forall\omega \end{aligned} \tag{21}$$

The constraint on $\|\mathcal{S}\|_\infty$ can be linearized analogously. It is important to note that the boundedness of the spectral norm $\|W\mathcal{U}\|$ does not necessarily guarantee the closed-loop stability for an arbitrary choice of $\widetilde{Z}$. The stability condition is presented in the following theorem:

Theorem 1: A feasible solution $K(s)$ to the optimization problem in (21) guarantees the closed-loop stability if

(a) $\widetilde{Z}$ is chosen as: $\widetilde{Z} = (I+G\widetilde{K})(j\omega\widetilde{K}_I - A)$, where $\widetilde{K}(s) = C(js\widetilde{K}_I - A)^{-1} + D$ stabilizes the closed-loop system.

(b) The number of RHP (Right-Half Plane) poles of $K(s)$ is equal to that of $\widetilde{K}(s)$

(c) $K(s)$ and $\widetilde{K}(s)$ share the same poles on the imaginary axis.

Proof: The proof is omitted to save space.

In order to be able to solve the problem, the semi-infinite sensitivity constraints are sampled at a reasonably large set of frequencies $\omega_k \in [\omega_1, \omega_2, \ldots, \omega_N]$. This design problem is then solved using an iterative approach. In order to start the iteration, a stabilizing initial controller $\widetilde{K}$ must be provided. For a stable plant, a stabilizing controller can be found by choosing the entries of K_P small and the entries of K_I large enough. Then, the following steps are repeated. First, the optimization problem is formulated using $\widetilde{Z} = Z^{curr}$ where Z^{curr} is the value of Z using the initial controller. Then, the optimization problem is solved and the controller coefficient matrices are updated and used to initialize the next iteration. The iteration can be halted as soon as the change in the objective function is small enough.

IV. Simulation Example

We used the method presented in section III to calculated a DAPI-controller for a test grid, and validated its performance in simulation. The results are compared to those of a classical droop controller, with the droop gains being equal to the proportional gains of the DAPI controller. The simulation was performed in Simulink using the Simpower toolbox. We based our grid model on the three-phase islanded Subnetwork 1 of the CIGRE benchmark medium voltage distribution network [18]. The network is a meshed network consisting of 11 buses (see Fig. 5).

The following modifications are made compared to the original system: We only consider 3 battery storage units connected to buses 5, 9 and 10. The photovoltaics are assumed to operate in maximum power point tracking mode and are absorbed into the loads. The loads at buses 1, 5, 9 and 10 were neglected. Since the grid runs in islanded mode, the loads and power ratings of the generation units were scaled such that nominal generation and load is at an equilibrium. To prevent the dynamics from being dominated by a single VSI, the power ratings are in a similar range for all three units. In Simulink, the inverters were modeled as ideal voltage sources following the dynamics described in section II-B. The grid parameters are listed in table I. The sensor dynamics H_L are assumed to be a first-order low-pass filter with time constants τ_L^{VSI}.

We assume a full communication graph, meaning that all three VSIs are able to communicate directly with each other. For our design problem we chose $\gamma_s = 2.4$, which is equal to the maximum of the sensitivity norm of the droop controller. It should be noted that the plant G used for the design contained 462 states, mostly introduced due to numerical errors in Matlab. While this number would be prohibitively large for classical control design methods, which generally need a minimal realization, the presented approach only requires the frequency response of the plant, and is therefore not affected by this problem. It would in fact also be possible to directly use the measured frequency response of the plant, without needing a parametric model. This is an important advantage in power grids, where the grid parameters and structure are often not well known.

TABLE I: Test Grid Parameters

Base Values	S_{base} = 4.75 MVA, U_{base} = 20 kV, f = 50 Hz
Batteries	
bus	[5 9 10]
$\bar{P}^{\text{VSI}}$	[-0.2 0.3 0.15] pu
k_p^{VSI}	[0.1 0.067 0.133] $\frac{\text{Hz}}{\text{pu}}$
k_i^{VSI}	[0.0151 0.0165 0.0214] $\frac{\text{Hz}\cdot\text{s}}{\text{pu}}$
τ_θ^{VSI}	[0.0002 0.0002 0.0002]
τ_L^{VSI}	[0.01 0.01 0.01]
Loads	
bus	[3 4 6 7 8 11]
$\bar{P}^{\text{load}}$	[0.05 0.0432 0.055 0.0077 0.0588 0.0331] pu

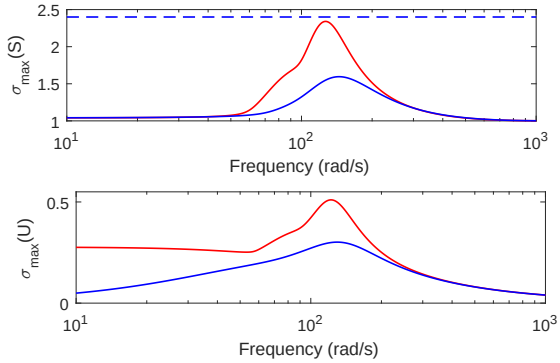

Fig. 6: The maximum singular values of $\mathcal{S}$ and $\mathcal{U}$; The solid red: droop controller, solid blue: DAPI controller

The controller is initialized with $K_I = \text{diag}([1, 1, 1])$ and the weighting frequency function is :

$$W(j\omega) = \begin{cases} 10, & \text{if } \omega \leq 10. \\ 1, & \text{otherwise.} \end{cases} \tag{22}$$

The algorithm converged to the final value within 47 iterations. The final gains of K_I are listed in table I. A comparison of the sensitivities for the droop and DAPI controller is shown in Fig. 6. A comparison of the frequency transients after a load step between the droop and DAPI controller is given in Fig. 7. At time 1 s the power drawn by the load at bus 3 was doubled. One can see that the DAPI controller returns the frequency to the nominal value of 50 Hz within less than 0.1 s and also provides an improved transient response.

V. Conclusions

We have presented a way to create a dynamic phasor model of the frequency dynamics of an inverter-based power grid that can readily be used for control design. We also presented a novel multivariable, fixed-structure frequency-domain control design approach. We have then demonstrated its potential by using the dynamic phasor model to design a distributed proportional-integral controller for an inverter-based microgrid. This control architecture serves to combine

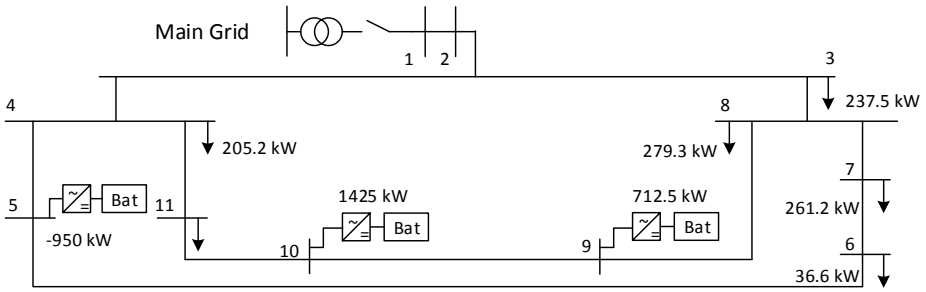

Fig. 5: Model adapted from [18] with 11 buses, 3 inverter-interfaced batteries and 6 loads. The sign ↓ denotes the loads.

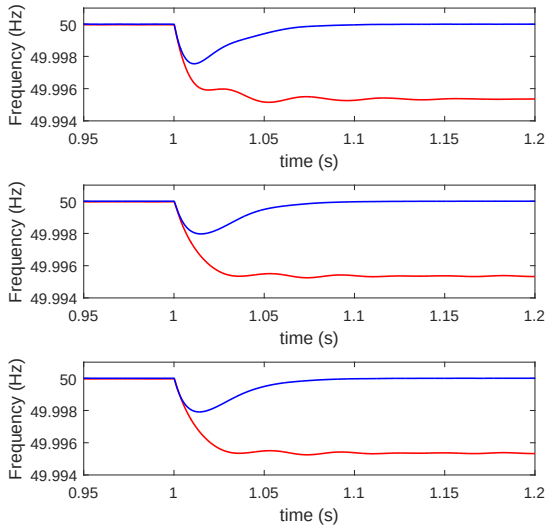

Fig. 7: Frequency transients after load change; red line: droop controller, blue line: DAPI controller.

droop control and secondary control, which significantly increases the bandwidth of secondary control while maintaining proportional power sharing. We have shown that the presented control design approach guarantees closed-loop stability while satisfying various performance goals.

References

[1] J. Guerrero, J. Vasquez, J. Matas, L. Vicuna, and M. Castilla. Hierarchical control of droop-controlled AC and DC microgrids - A general approach toward standardization. *IEEE Trans. on Industrial Electronics*, 58(January):158–172, 2011.

[2] F. Dörfler, J. Simpson-Porco, and F. Bullo. Breaking the hierarchy: distributed control & economic optimality in microgrids. *IEEE Trans. on Control of Network Systems*, (DOI 10.1109/TCNS.2015.2459391), 2016.

[3] P. Kundur, N. J. Balu, and M. G. Lauby. *Power system stability and control*, volume 7. McGraw-hill New York, 1994.

[4] A. Bidram and A. Davoudi. Hierarchical structure of microgrids control system. *Smart Grid, IEEE Transactions on*, 3(4):1963–1976, 2012.

[5] A. Tsikalakis and N. Hatziargyriou. Centralized control for optimizing microgrids operation. In *Power and Energy Society General Meeting, 2011 IEEE*, pages 1–8. IEEE, 2011.

[6] M. Savaghebi, A. Jalilian, J. Vasquez, and J. Guerrero. Secondary control scheme for voltage unbalance compensation in an islanded droop-controlled microgrid. *Smart Grid, IEEE Transactions on*, 3(2):797–807, 2012.

[7] J. Simpson-porco, F. Dörfler, and F. Bullo. Synchronization and power sharing for droop-controlled inverters in islanded microgrids. *Automatica*, 1(February):1–11, 2013.

[8] Q. Shafiee, J. Guerrero, and J. Vasquez. Distributed secondary control for islanded microgrids - A novel approach. *IEEE Trans. on Power Electronics*, 29(2):1018–1031, 2014.

[9] J. Vasquez, J. Guerrero, M. Savaghebi, J. Eloy-Garcia, and R. Teodorescu. Modeling , Analysis , and Design of Parallel Three-Phase Voltage Source Inverters. *IEEE Trans. on Industrial Electronics*, 60(4):1271–1280, 2013.

[10] J. Schiffer, R. Ortega, A. Astolfi, J. Raisch, and T. Sezi. Conditions for stability of droop-controlled inverter-based microgrids. *Automatica*, 50(10):2457–2469, October 2014.

[11] C. DeMarco, C. Baone, Y. Han, and B. Lesieutre. Primary and secondary control for high penetration renewables. *The Future Grid to Enable Sustainable Energy Systems*, 2012.

[12] M. Sadabadi, A. Karimi, and H. Karimi. Fixed-order decentralized/distributed control of islanded inverter-interfaced microgrids. *Control Engineering Practice*, 45:174–193, 2015.

[13] X. Guo, Z. Lu, B. Wang, X. Sun, L. Wang, and J. Guerrero. Dynamic phasors-based modeling and stability analysis of droop-controlled inverters for microgrid applications. *IEEE Trans. on Smart Grid*, 5(6):2980–2987, 2014.

[14] K. De Brabandere. *Voltage and Frequency Droop Control in Low Voltage Grids By Distributed Generators with Inverter Frond-End*. PhD thesis, Katholieke Universiteit Leuven, FACULTEIT INGENIEURSWETENSCHAPPEN, 3001 Leuven, Belgium, 2006.

[15] P. Apkarian and D. Noll. Nonsmooth H_∞ synthesis. *IEEE Trans. on Automatic Control*, 51(1):71–86, 2006.

[16] J. V. Burke, D. Henrion, and A. S. Lewis M. L. Overton. HIFOO : a MATLAB package for fixed-order controller design and H_∞ optimization. In *Fifth IFAC Symposium on Robust Control Design, Toulouse*, 2006.

[17] S. Boyd, M. Hast, and K. J. Åström. MIMO PID tuning via iterated LMI restriction. *International Journal of Robust and Nonlinear Control*, 26(8):1718–1731, 2016.

[18] K. Rudion, A. Orths, Z.A. Styczynski, and K. Strunz. Design of benchmark of medium voltage distribution network for investigation of DG integration. *2006 IEEE Power Engineering Society General Meeting*, page 6, 2006.